Distinct structural features associated with conformational epitopes of amyloid β fibrils revealed using mathematical geometric measures

Masumi Sugiyama
Hiroshima University
Shang-Te Danny Hsu
Academia Sinica
Eleni Panagiotou
Arizona State University
Shin-ichi Tate
tate@hiroshima-u.ac.jp

Hiroshima University

Article

Keywords:

Posted Date: April 17th, 2026

DOI: https://doi.org/10.21203/rs.3.rs-9285528/v1

Additional Declarations: No competing interests reported.

Article

Distinct structural features associated with conformational epitopes of amyloid β fibrils revealed using mathematical geometric measures

Masumi Sugiyama[1], Shang-Te Danny Hsu[1,2], Eleni Panagiotou[1,6] and Shin-ichi Tate[1,3,4,5,*]

[1] International Institute for Sustainability with Knotted Chiral Meta Matter (WPI-SKCM[2]), Hiroshima University, 1-3-1 Kagamiyama, Higashi-Hiroshima 739-8526, Japan
[2] Institute of Biological Chemistry, Academia Sinica, Taipei 11529, Taiwan
[3] Department of Mathematical and Life Sciences, Graduate School for the Integrated Sciences for Life, Hiroshima University, 1-3-1 Kagamiyama, Higashi-Hiroshima 739-8526, Japan
[4] Meiji Institute for Advanced Study of Mathematical Sciences (MIMS), Meiji University, 4-21-1 Nakano, Nakano-ku, Tokyo 164-8525, Japan
[5] Graduate School of Medical Life Science, Yokohama City University, 1-7-29 Suehiro-cho, Tsurumi-ku, Yokohama 230-0045, Japan
[6] School of Mathematical and Statistical Sciences, Arizona State University, Tempe, AZ 85281, USA

*Corresponding author: Shin-ichi Tate (tate@hiroshima-u.ac.jp)

Abstract

Monoclonal antibodies (mAbs) targeting the key pathogenic protein amyloid β (Aβ) peptide represent a promising therapeutic approach for treating Alzheimer's disease (AD). Anti-Aβ mAbs are classified by their affinity to different states of Aβ, such as monomers, oligomers, protofibrils, and fibrils. Recently developed second-generation mAbs, which effectively remove Aβ plaques from the AD patients' brains, exhibit specific avidity for Aβ oligomers, protofibrils, and fibrils. These mAbs target epitopes in specific conformations displayed on Aβ oligomers, protofibrils, or fibrils; thus, they are called *conformational epitopes.* However, the structural features of conformational epitopes are poorly understood. Here, we proposed geometric measures based on the mathematically defined writhe. We found that the conformational epitopes of Aβ in the 69 fibrils show distinctive geometric features compared to the other regions of Aβ, as evidenced by outlying values of the geometric measures. Mapping regions with higher measure values identifies potential conformational epitopes across various fibril forms. Results showed that some fibril forms exhibit geometrically distinct regions within the fibril structures, suggesting that these fibrils are less accessible to mAbs, impairing therapeutic effects targeting them. Our geometric measures reveal visually unidentified structural features of conformational epitopes in polymorphic Aβ fibrils, which relate to mAbs binding.

Keywords:
amyloid β fibrils, conformational epitope, monoclonal antibody therapy, Alzheimer's disease, mathematical writhe

Introduction

Alzheimer's disease (AD) is the most common cause of dementia. In AD pathology, deposition of the amyloid β (Aβ) peptide in the brain is a core event[1,2]. Aβ forms extracellular plaques and oligomers that can spread the disease via cell-to-cell propagation[3]. The accumulation of Aβ deposits considerably provokes tau pathology, eventually causing neuronal loss[1,3]. Over 100 therapeutic agents are being tested in clinical trials for AD. Among the most promising ones are disease-modifying anti-Aβ monoclonal antibodies (mAbs)[4-6]. Anti-Aβ mAbs are classified by their affinity to diverse forms of Aβ, such as monomers, oligomers, fibrils, and protofibrils[5]. First-generation mAbs targeting monomeric Aβ, such as solanezmab, bapineuzumab, and crenezumab, have not shown substantial therapeutic benefits in clinical trials[1,5]. Second-generation mAbs, including aducanumab, lecanemab, donanemab, and gantenerumab, that target pathogenic Aβ species, such as oligomers, protofibrils, and fibrils, reportedly reduce Aβ deposition and slow cognitive decline[1,4,5].

In pathogenic Aβ species, epitopes are displayed in specific conformations, and second-generation mAbs target these *conformational epitopes*[5,7,8]. However, the structural features of conformational epitopes are poorly understood[5,7,9], preventing the design of an immunisation strategy to develop efficient anti-Aβ mAbs that can selectively target pathogenic Aβ species rather than abundant healthy Aβ species[9-11]. The polymorphism of Aβ fibrils is a considerable obstacle in passive immunotherapy [9,12]. An mAb selectively targeting a conformational epitope displayed on one fibril type should be ineffective at binding to other fibril forms.

We have previously reported that protein-binding surfaces tend to be geometrically distinct[13-15]. Here, we devised geometric measures using the mathematically defined writhe to characterise the conformational epitopes of Aβ in 69 fibril forms and to identify potential conformational epitopes among them. We found that conformational epitopes exhibit distinctive geometric features across various fibril forms, as identified by outlying values in our geometric measures. We found that the potential epitope regions characterised by high geometric measure values are close in sequence position to those determined biochemically. The results also demonstrated that polymorphism in Aβ fibrils masks potential epitopes in certain fibril forms, limiting mAbs' access to them and thereby probably reducing the clinical benefit of AD immunotherapy.

Results

Geometric features of protein structure revealed using "writhe"

In mathematical topology, particularly knot theory, the so-called writhe, which is calculated from 3D coordinates of knotted rings without using any projections and algebraic invariants, is used as a numerical measure to classify knot structures[16-18]. Writhe quantifies the geometrical entanglement of a ring with itself, as seen in plectoneme-like double-folding ring polymers[19]. Writhe measures the entire ring entanglement, while 'local writhe' shows the distribution of segment-wise local entanglement over a ring, thus providing a 1D local entanglement profile[18]. This profile can classify knots, threading, and entanglements[18,20-22], implying that the local writhe–derived profile over a ring represents the geometric features underlying topology; in other words, it retains the geometric information equivalent to what is represented by topological invariants and knot polynomials [20,21]. In knot theory, writhe and local writhe are applied to explore ring structures[18,19,22]. However, such an application is not limited to rings. We can take advantage of local writhe's sensitivity to the entangled local structure to explore conformations of open-ended polymers, such as proteins[13-15,23,24].

Here, we used local writhe as a basic metric to explore geometric features of conformational epitopes of Aβ across 69 different fibrils, leveraging its sensitivity to local self-entanglement. We detailed the structural features using local writhe that underlie the geometric measures used in this work.

The local writhe for a protein is based on the residue-to-residue writhe, Wr(*s,t*), which is defined for a pair of residues positioned at *s* and *t* in a polypeptide; the corresponding residue positions are denoted as γ(*s*) and γ(*t*), respectively (Fig. 1a). Wr(*s,t*) is calculated using three vectors on the polypeptide chain: two unit tangent vectors dγ(*s*) and dγ(*t*), at γ(*s*) and γ(*t*) positions, respectively, and the inter-residue vector ***r*** connecting γ(*s*) and γ(*t*), ***r*** = γ(*t*) − γ(*s*), as shown in Fig. 1a. The vector ***v*** is the outer product of the two tangent vectors, ***v*** = dγ(*t*) × dγ(*s*), as shown in Fig. 1b. Wr(*s,t*) is then defined using the inner product of the vectors ***v*** and ***r*** as $\mathrm{Wr}(s,t) = \boldsymbol{v}\cdot\boldsymbol{r}/|\mathbf{r}|^3 = \sin\theta\cos\phi\,/|\boldsymbol{r}|^2$, where θ is the angle between the two tangent vectors, dγ(*s*) and dγ(*t*), while ϕ is the angle between the vectors ***v*** and ***r*** (Fig. 1b).

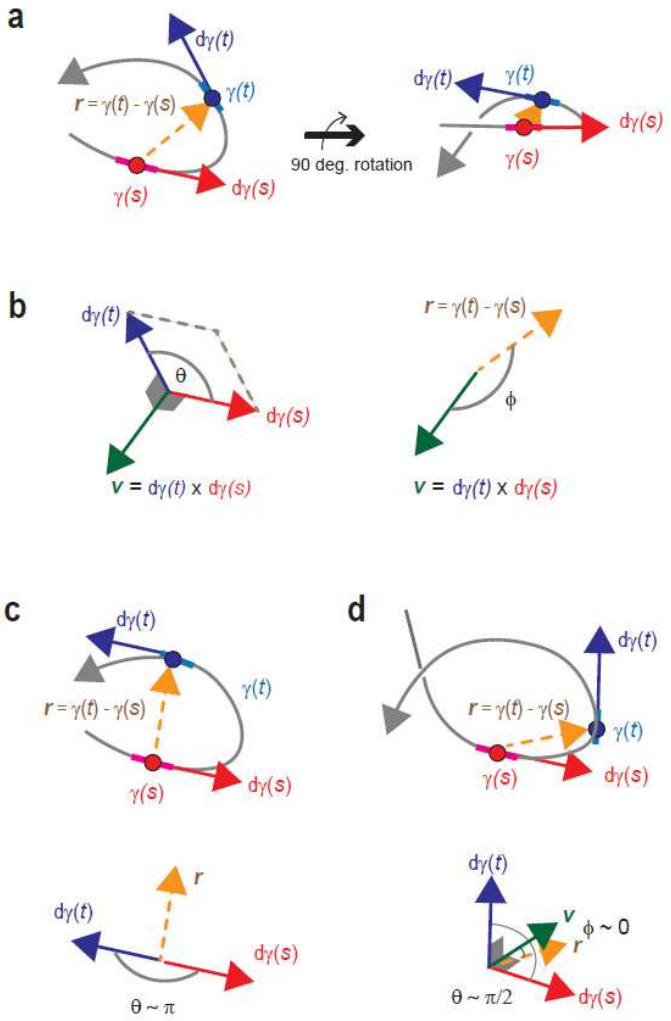

Fig. 1. Three vectors defining writhe. (**a**) The vectors on a loop region of a polypeptide. The grey curve represents the polypeptide. Cartesian coordinates for residues *s* and *t* are described by γ(*s*) and γ(*t*) positions, respectively. Unit tangent vectors at γ(*s*) and γ(*t*) positions are denoted as dγ(*s*) and dγ(*t*), respectively. The vector connecting the two residue positions is defined as ***r*** = γ(*t*) − γ(*s*). Writhe has a large value when the loop is twisted, as shown in the cartoon on the right. (**b**) The vector ***v*** is the outer product of the unit tangent vectors, ***v*** = dγ(*t*) × dγ(*s*). The two angles, θ and ϕ, are defined by the angles between dγ(*s*) and dγ(*t*) and those between ***v*** and ***r***, respectively. (**c**) Local writhe between two residue positions, Wr(*s,t*), is proportional to the inner product of vectors ***v*** and ***r***. If the two residues *s* and *t* are on a planar loop, angle θ is close to 0; thus, Wr(*s,t*) is nearly 0. (d) Residues *s* and *t* on a twisted loop make θ and ϕ close to π/2 and 0, respectively.

Wr(s,t) represents local entanglement of the polypeptide. If the tangent vectors dγ(s) and dγ(t) in a loop are nearly antiparallel (i.e. the loop is in a planar conformation), $\boldsymbol{v}$ is close to 0, making Wr(s,t) nearly 0 (Fig. 1c). However, if the loop forms a self-winding conformation, and residue t is at the centre of a tight loop, the two tangent vectors dγ(s) and dγ(t) can be closely perpendicular to each other (Fig. 1d), in which the vectors $\boldsymbol{v}$ and $\boldsymbol{r}$ can be closely parallel, giving Wr(s,t) nearly the largest value for the residues distant at $\boldsymbol{r}$, $1/|\boldsymbol{r}|^2$ (Fig. 1d).

The residue-wise local writhe for a residue s, Wr(s), is defined using the sum of Wr(s,t) collected for all other t residues out of residue s in the protein: $\mathrm{Wr}(s) = \frac{1}{2\pi}\sum_i \mathrm{Wr}(s,i)$, where i denotes the residue number excluding the residue s. In practice, we use the "window" segment l with a finite number of residues, n, instead of a single residue at s to smooth out short-range variations of the residue-wise Wr(s) value. The segment-wise local writhe, Wr(l), is defined as

$$\mathrm{Wr}(l) = \frac{1}{2\pi}\sum_j \mathrm{Wr}(j) = \frac{1}{2\pi}\sum_{j\in l}\sum_i \mathrm{Wr}(j,i) \quad (1)$$

where j represents the residue number in fragment l (Fig. 2a). By moving the window along the protein sequence, we can obtain a 1D local writhe profile[15,18] (Fig. 2a). Note that Wr(l) represents the chirality and magnitudes of entanglement. Therefore, Wr(l) takes positive and negative values, depending on the self-winding chirality. The geometric measure we introduced here does not consider the winding chirality but only the absolute magnitude, which we designate as *absolute local writhe*, absWr(l). The absWr(l) value increases when segment l is part of a self-wound loop, making it a visible metric for local conformational entanglement (Fig. 2b).

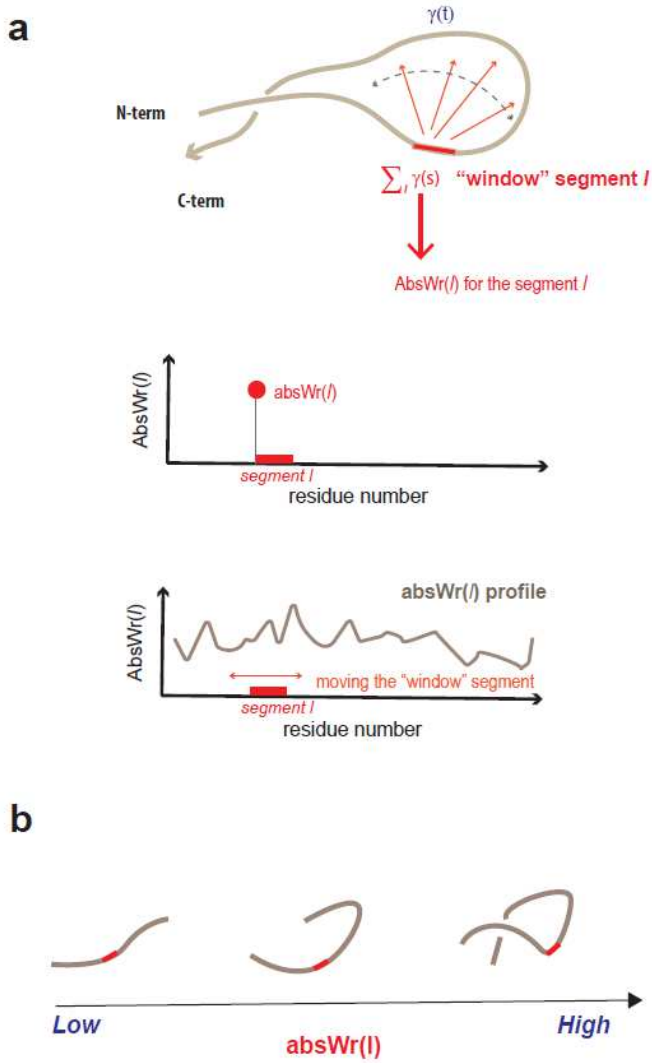

Fig. 2. Segment-wise local writhe. (**a**) Segment *l* comprises a finite number of residues. For each residue *s* in segment *l*, Wr(*s*) is defined as the sum of the residue-wise writhes, Wr(*s,t*), over all residues *t* except *s*. The local writhe Wr(*l*) is defined as the sum of Wr(*s*) over the residues in segment *l*. The absolute value of Wr(*l*), denoted absWr(*l*), was used here (top). Each segment *l* in an Aβ fibril exhibits an absWr(*l*) at the segment location: the value is plotted at the position of the first residue of segment *l* (middle). Moving segment *l* along the residue in Aβ exhibits the absWr(*l*) profile (bottom). (**b**) Schematic drawing demonstrating the relationship between the local peptide conformation (grey curve) and the absWr(*l*) value. Segment *l* (red bar) embedded in a twisted or entangled loop exhibits a higher absWr(*l*) value. Aβ: amyloid β.

Absolute local writhe profiles of Aβ across 69 fibrils

The absolute local writhe of Aβ in 69 fibrils demonstrated that each Aβ shows obvious variations in absWr(*l*), along with the residues (Fig. 3 and Supplementary Fig. S2). The window segment *l* contained four residues. Note that the number of residues experimentally observed in Aβ was different in each fibril (Supplementary Table S1). Each fibril deposited in the Protein Data Bank (PDB) contains a different number of Aβ peptides (Supplementary Table S2). Some fibrils contain Aβ in different conformations, while others contain Aβ in the fibrils in the same conformation; this difference is attributed to the experimental procedure adopted in solving the fibril structures: 42 out of the 69 fibrils

have the identical Aβ structure (Supplementary Table S3).

The reported sequence positions of conformational epitopes of the four representative second-generation mAbs are the following:

- Gantenerumab: Aβ residues 3–11 and 18–27 [5,25]
- Lecanemab: Aβ residues 1–16 and 21–29 [5,26]
- Aducanumab: Aβ residues 3–7 [9,27,28]
- Donanemab: Aβ residues 3–13 [9,27,28]

The conformational epitopes are located in two different parts of Aβ: the N-terminal region of around residues 1–15, and the middle part around residues 20–30. Supplementary Fig. S1 shows the locations plotted alongside the Aβ residues in different fibrils.

Representative local writhe profiles are shown in Figs. 3a–c. Aβ in fibril 7q4m (12–42), where 7q4m is the PDB accession code with observed Aβ residues 12–42, shows five regions with high absWr(l) values, which are greater than average absWr(l) + one half of standard deviation (σ); the regions are marked on the Aβ structures in the fibril (Fig. 3a). Note here that absWr(l) value for a four-residue segment is plotted at the first residue of the segment (Fig. 2a, middle). In the case of the 7q4m (12–42) profile, the residue 16 with high absWr(l) indicates that the segment of residues 16–19 is in a substantially entangled state (Fig. 3a, left); thus, the four residues 16–19 are marked on the structure (Fig. 3a, right). Because the residues overlap among the segments with high absWr(l) values, the number of marked structured regions on the structure becomes less than the marked regions in the absWr(l) profile.

Aβ in fibril 9jb2 (1–42) has five regions with high absWr(l) values (Fig. 3b), and Aβ in fibril 9jaz (9–42) has also five regions with high absWr(l) values (Fig. 3c). A visual inspection of the structures did not readily identify the local entanglement in these Aβ peptides, but local writhe picked them up. Aβ in other fibrils share similar absWr(l) distributions (Supplementary Fig. S2). The average absWr(l) values collected for each Aβ residue in 69 fibrils demonstrated that there are four regions with high absWr(l) values in the profile (Fig. 3d), corresponding to three geometrically distinct segments in the Aβ structure: residues 6–11, 21–31, and 35–40. The N-terminal and middle regions roughly match the conformational epitopes (Supplementary Fig. S1), which suggests that the conformational epitopes are characterised by their local conformation with high absWr(l). It is interesting to point out that the geometrically distinct C-terminal part of the Aβ, residues 35–40, should be a hidden conformational epitope.

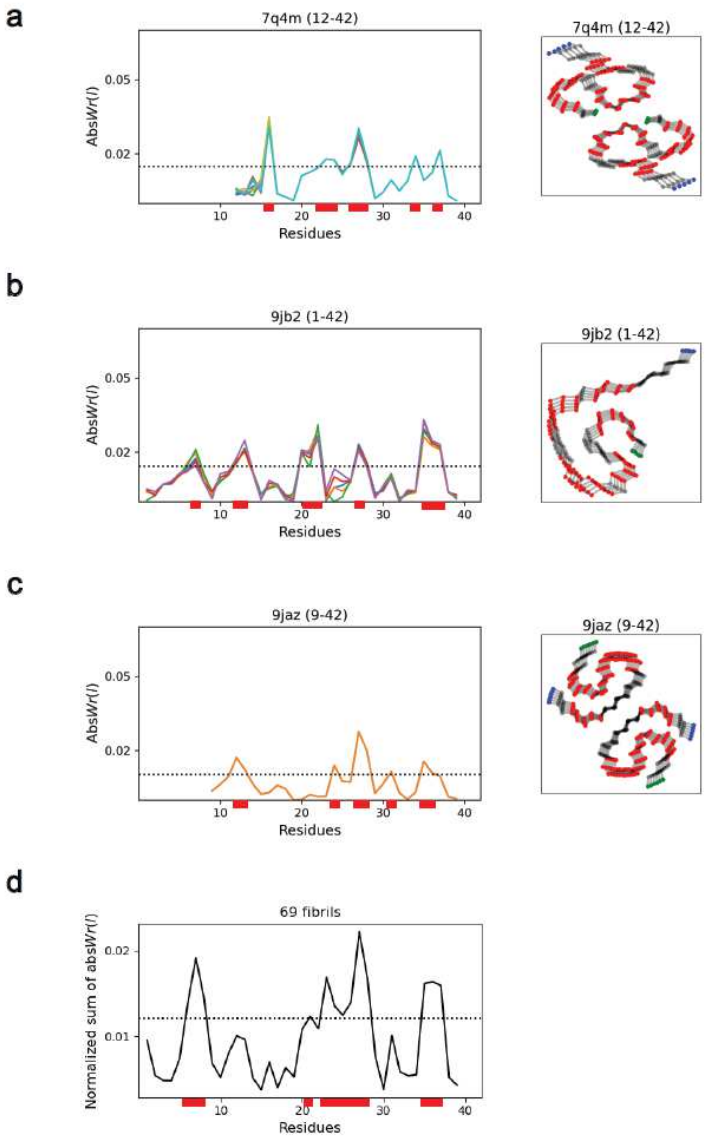

Fig. 3. Distribution of the absolute local writhe, absWr(*l*), for all Aβ peptides in three different fibrils (left column) and corresponding Aβ structures (right column). The different colours in each panel represent the different Aβ peptides in the fibril. The dotted line indicates the value corresponding to the average absWr(*l*) + one-half of the standard deviation for Aβ peptides in each fibril. The segment size was set to 4 (a 4-residue window). The red bars indicate the first residues of the four-residue segments showing absWr(*l*) values greater than the threshold value indicated by dotted lines, which constitute local segments geometrically distinct from the other regions of Aβ. The corresponding parts are marked in red on the Aβ structures. (**a**) Fibril 7q4m (12–42) has three geometrically distinct regions: Aβ residues 16–19, 23–31, and 34–40 (threshold: 0.015). (**b**) Fibril 9jb2 (1–42) has four geometrically distinct regions: Aβ residues 7–16, 20–30, and 35–40 (threshold: 0.014). (**c**) Fibril 9jaz (9–42) has three geometrically distinct regions: Aβ residues 12–16, 24–34, and 35–40 (threshold: 0.010). The Aβ peptides in fibril 9jaz (9–42) are in the same conformation. (**d**) Distribution of average absWr(*l*) values of all Aβ peptides in 69 fibrils. There are three geometrically distinct regions: Aβ residues 6–11, 21–31, and 35–40 (threshold: 0.012). The value at each residue position is normalised by the number of Aβ residues observed in 69 fibrils. Aβ: amyloid β.

Local writhe for each conformational epitope across 69 fibrils

We compared the absWr(l) values of the conformational epitopes recognised by the four mAbs, aducanumab, lecanemab, donanemab, and gantenerumab (Table 1). The absWr(l) value depends on the number of Aβ residues in the epitope segment l. Therefore, we compared the absWr(l)/N values, where N is the number of Aβ residues constituting the epitope. We also averaged the absWr(l)/N values over the Aβ peptides in each fibril. The *average absolute local writhe* measure, aaWr(l), is defined as

$$\mathrm{aaWr}(l) = \frac{\sum_{i=1}^{m} \mathrm{absWr}^{i}(l)/N}{m} \qquad (2)$$

where m is the number of Aβ peptides in the fibril and $\mathrm{absWr}^{i}(l)$ is the absWr(l) value for the epitope in the i-th Aβ peptide in the fibril.

We classified fibrils into four groups, L0, L1, L2, and L3, based on the aaWr(l) value for each fibril (Table 1). For the lecanemab (21–29) epitope, aaWr(l) > 0.005 (L2 and L3 groups) in 36 (52%) out of 69 different fibril structures , showing that the epitope located in the middle of the Aβ peptide exhibits higher self-entangled conformations in the fibrils (Table 1). Similarly, for the gantenerumab (18–27) epitope, aaWr(l) > 0.005 (L2 group) in 24 (35%) out of 68 fibrils (Table 2). The averaged absWr(l) profile (Fig. 3d) supports that the lecanemab (21–29) and gantenerumab (18–27) epitopes in the fibrils contain local structures with substantial entanglement.

Notably, for the aducanumab (3–7) epitope, aaWr(l) > 0.01 (L3 group) in only one fibril (PDB code 2m4j), as shown in Table 1. The aducanumab (3–7) epitope in the Aβ peptide in fibril 2m4j (1–40) has a different geometry than the corresponding segments in other fibrils (Supplementary Fig. S3): the Cα-connecting vector from residues 3 to 4 orients almost perpendicular to the other Cα-connecting vectors, which are mostly in plane. In contrast, in all other cases, all Cα-connecting vectors are mostly planarly arranged (Supplementary Fig. S3). Notably, even at its N-terminal location, the aducanumab (3–7) epitope exhibits a substantially entangled conformation.

These results demonstrate that Aβ regions exhibiting substantial local entanglement are located within conformational epitopes regardless of polymorphic fibrils (Fig. 3 and Table 1).

Table 1: Mean aaWr(*l*) values for each conformational epitope of the Aβ peptide in the 69 fibrils.

Epitope in Aβ	Mean aaWr(*l*) [a)]	Number of structures [b)]	Classes of aaWr(*l*) value [c)]			
			L0	L1	L2	L3
Lecanemab (1–16)	0.0035 ± 0.0023	18	5	8	5	0
Lecnemab (21–29)	0.0055 ± 0.0031	69	9	24	30	6
Gantenerumab (3–11)	0.0038 ± 0.0030	19	8	5	5	1
Gantenerumab (18–27)	0.0040 ± 0.0024	68	18	26	24	0
Docanemab (3–13)	0.0036 ± 0.0030	19	6	7	6	0
Aducanumab (3–7)	0.0012 ± 0.0025	19	16	2	0	1

a) Mean aaWr(*l*) value ± standard deviation for the aaWr(*l*) values over the fibrils that contain the entire residues in the epitope.

b) Number of fibril structures used in calculating the mean aaWr(*l*) value. The fibril structures were not used in the analysis unless all the epitope residues were included in the Aβ peptide of the fibrils.

c) The fibril structures were classified value into four categories based on each aaWr(*l*) value: L0: aaWr(*l*) $\leq$ 0.002, L1: 0.002 < aaWr(*l*) $\leq$ 0.005, L2: 0.005 < aaWr(*l*) $\leq$ 0.010, L3: aaWr(*l*) > 0.010.

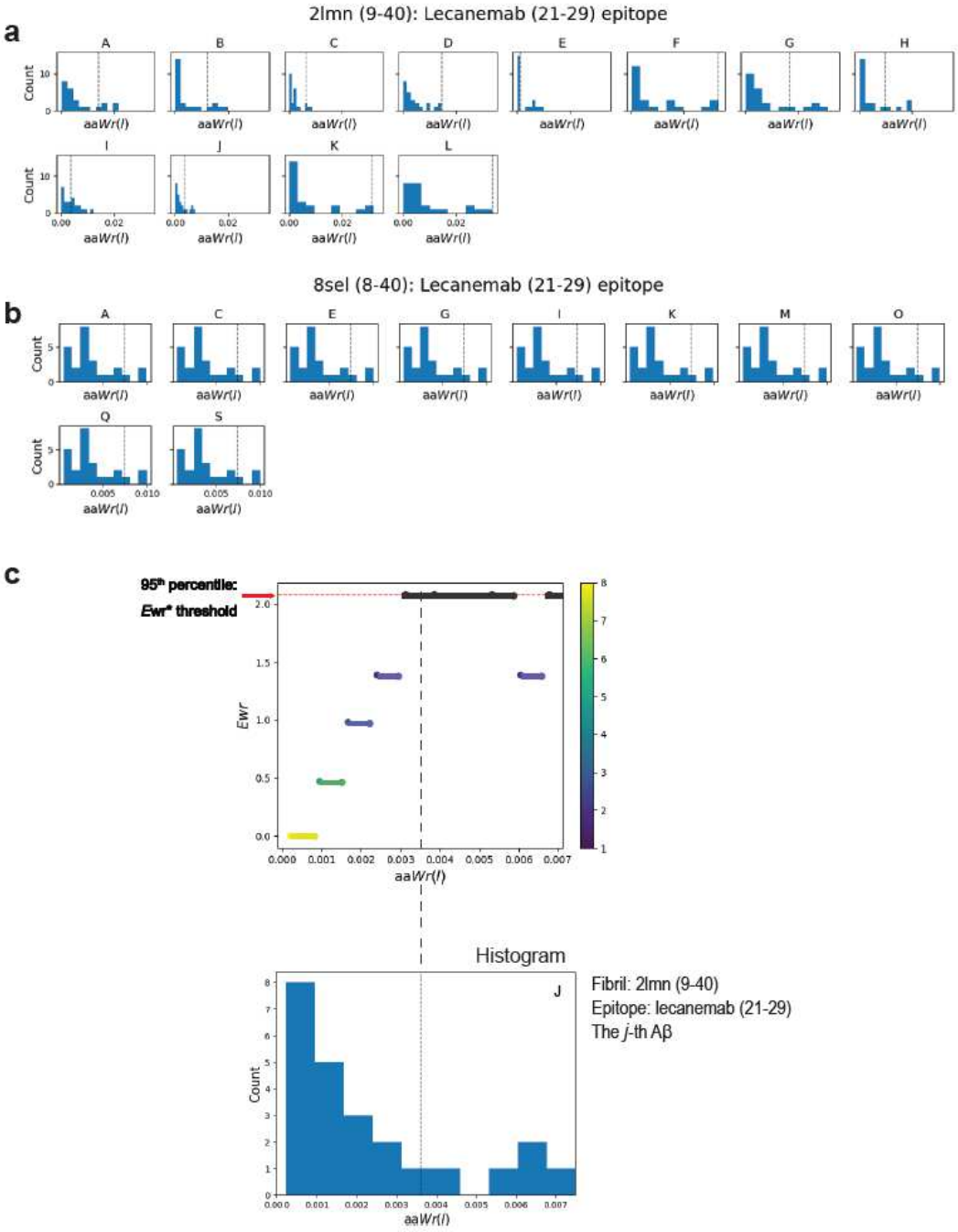

Fig. 4. Histograms of aaWr(l) values of Aβ peptides collected with a 9-residue window size corresponding to Aβ residues of the lecanemab (21–29) epitope for (**a**) fibril 2lmn (9–40) and (**b**) fibril 8sel (8–40). The dotted lines in the panels indicate the bin where the aaWr(l) of the lecanemab (21–29) epitope is involved. (**c**) Example of the local writhe energy, $E_{wr}(l)$, distribution obtained from one of the Aβ peptides (j-th peptide) in fibril 2lmn (9–40). Each $E_{wr}(l)$ value shown using a horizontal bar is determined by the count in each bin of the aaWr(l) histogram; the count is indicated by the colour of the horizontal bar. The red dotted horizontal line in the $E_{wr}(l)$ graph shows the 95th percentile value of $E_{wr}(l)$. The $E_{wr}(l)$ over this line is denoted as $E_{wr}(l)$*. The vertical black dotted line indicates the bin where the aaWr(l) value of the lecanemab (21–29) epitope falls. The corresponding bin includes one fragment; thus, the epitope shows the $E_{wr}(l)$* value. Aβ: amyloid β.

Conformational epitopes show outlying aaWr(*l*) values

We further examined where the epitope's aaWr(*l*) value falls among all aaWr(*l*) values within the same Aβ peptide. Here, we show representative results for Aβ in fibril 2lmn (9–40), analysed with a nine-residue window size corresponding to the Aβ residues in the lecanemab (21–29) epitope (Fig. 4a and Supplementary Table S2). Fibril 2lmn (9–40) contains 12 Aβ peptides (designated A–L). Fig. 4a displays an aaWr(*l*) histogram for each Aβ peptide in fibril 2lmn (9–40). The dotted lines indicate the aaWr(*l*) value for the lecanemab (21–29) epitope. The data show that the epitope's aaWr(*l*) value is distinct from the values of the other parts in the same Aβ peptide (Fig. 4a). Fibril 8sel (8–40) has 10 Aβ peptides (designated A–S), indicating that the lecanemab (21–29) epitope has an outlying aaWr(*l*) value (Fig. 4b).

For the lecanemab (21–29) epitope, 22 (32%) out of the 69 fibrils had at least one Aβ peptide with an aaWr(*l*) value above the 95th percentile (Table 2 and Supplementary Table S2), which we designated as an outlying aaWr(*l*) value, aaWr(*l*)*. For the lecanemab (1–16) epitope, 6 (33%) out of 18 fibrils had an Aβ peptide with aaWr(*l*)* (Table 2). The proportion of fibrils with Aβ peptides with aaWr(*l*)* for either the lecanemab (1–16) or the lecanemab (21–29) epitope was 39% (Table 2). The results suggest that geometric entanglement is a hallmark of the conformational epitope targeted by lecanemab.

The gantenerumab (18–27) epitope had Aβ with aaWr(*l*)* in 9 (13%) out of 68 fibrils (Table 2), fewer than those in the lecanemab (21–29) epitope. However, the gantenerumab (18–27) epitope had aaWr(*l*) values in the L2 group in 24 (35%) out of 68 fibrils (Table 1). This was similar to the lecanemab (21–29) epitope, for which aaWr(*l*) values were in the L2 group across 30 fibrils (Table 1). The gantenerumab (3–11) epitope did not show aaWr(*l*)* values in any fibrils (Table 2) but exhibited aaWr(*l*) values in the L2 group in 5 fibrils, which is the same number as for the lecanemab (1–16) epitope (Table 1). These results suggest that conformational epitopes are characterised by significant geometric entanglement, as shown by the higher aaWr(*l*) values, compared to other regions of Aβ.

Geometric uniqueness of conformational epitopes

We explored the geometric uniqueness of conformational epitopes relative to other regions of Aβ by introducing a new measure called *local writhe energy* (E_{wr}). E_{wr} is similar to our previously reported local topological free energy[15] — a measure of geometric uniqueness of a local conformation in a specific protein in reference to local segmental structures in a set of proteins in different folds. Both measures rely on writhe[13,14]. Here, 'geometric uniqueness' of a local structure means that the local segment of a protein takes the least probable geometry among a set of local conformations in the same Aβ peptide. $E_{\mathrm{wr}}(l)$ is defined for segment l (l-residue window) as

$$E_{\mathrm{wr}}(l) = \ln(N(H_{\mathrm{wr}})/N(P_{\mathrm{wr}})) \qquad (3)$$

where $N(H_{\mathrm{wr}})$ is the number of the fragments in the highest populated bin of the aaWr(*l*) histogram for an Aβ peptide, and $N(P_{\mathrm{wr}})$ is the number of fragments in a bin that includes the specific value aaWr(*l*) = P in the aaWr(*l*) histogram. $E_{\mathrm{wr}}(l)$ increases when the segment with the value of P falls in a bin with fewer segments in the aaWr(*l*) histogram (Fig. 4c). The size of segment l is set to the number of Aβ residues in the epitope in focus; for example, l was set to 9 to explore the conformational uniqueness of the lecanemab (21–29) epitope.

Figure 4c illustrates the case of the lecanemab (21–29) epitope in fibril 2lmn (9–40). The aaWr(*l*) for the epitope does not reach its highest value among the fragments in this specific Aβ peptide. However, the aaWr(*l*) value falls in one of the least populated bins of the aaWr(*l*) histogram, thus exhibiting the highest $E_{\mathrm{wr}}(l)$. We designated the $E_{\mathrm{wr}}(l)$ values over the 95th percentile as $E_{\mathrm{wr}}(l)$* (Fig. 4c). The lecanemab (21–29) epitope in fibril 2lmn (9–40) exhibited $E_{\mathrm{wr}}(l)$*, indicating that the epitope forms a unique entangled form in Aβ. The conformational uniqueness of the epitope should promote specific

recognition by mAbs.

The segment with aaWr(l)* does not always exhibit $E_{wr}(l)$*, as shown for fibril 2lmn (9–29) with the lecanemab (21–29) epitope (Fig. 4c). The local entanglement of the epitope is characterised by either its degree of entanglement, aaWr(l)*, or its unique entangled conformation, $E_{wr}(l)$*. The aaWr(l) histograms for each Aβ peptide in every fibril with the window size corresponding to each epitope are provided in Supplementary Fig. S4.

For the lecanemab (1–16) epitope, 2 (3%) out of the 69 fibrils were identified using E_{wr}(l)*, whereas 6 were identified using aaWr(l)* (Table 2). For the lecanemab (21–29) epitope, 25 and 22 fibrils were identified using E_{wr}* and aaWr(l)*, respectively (Table 2). For the donanemab (3–13) epitope, one fibril was identified by $E_{wr}(l)$* and none were identified using aaWr(l)* (Table 2). The lecanemab (21–29) epitope in the Aβ peptide had a distinctive geometry characterised by either aaWr(l)* or $E_{wr}(l)$* in 35 (51%) out of 69 fibrils. For the lecanemab (1–16) epitope, 7 (39%) out of 18 fibrils contained the epitope in a distinct geometry. In addition, 40 (58%) out of 69 fibrils featured outlier geometries of the lecanemab (1–16) or the lecanamab (21–29) epitope. For the gantenerumab (3–13) or the gantenerumab (18–27) epitope, this number was 26 (38%) out of 68 fibrils (Table 2). These results demonstrate that the outlier geometric features characterised by aaWr(l)* (entanglement) or $E_{wr}(l)$* (uniqueness) are associated with conformational epitopes.

Table 2: The number of fibrils containing Aβ peptides with outlying geometric values for various epitopes.

epitope	Number of fibrils [a]	Aβ with aaWr(l)* [b]			Aβ with Ewr(l)* [c]			Aβ with aa Wr(l)* or Ewr(l)* [d]		
Lecanemab (1–16)	18	6	(33%)	27/69 (39%)	2	(11%)	27/69 (39%)	7	(39%)	40/69 (58%)
Lecanemab (21–29)	69	22	(32%)		25	(36%)		35	(51%)	
Gantenerumab (3–11)	19	0	(0%)	13/68 (13%)	1	(5%)	23/68 (34%)	1	(5%)	26/68 (38%)
Gantenerumab (18–27)	68	9	(13%)		22	(32%)		25	(37%)	
Docanemab (3–13)	19	0	(0%)	n.a.	4	(21%)	n.a.	4	(21%)	n.a.
Aducanumab (3–7)	19	0	(0%)	n.a.	0	(0%)	n.a.	0	(0%)	n.a.

a) Number of fibrils that contain the Aβ peptides with all epitope residues in concern.
b) Number of fibrils that contain at least one Aβ peptide with aaWr(l)* (the aaWr(l) value is above the 95th percentile) with its percentage ratio among the fibrils in parentheses. In the third column, the number of fibrils that contain at least one Aβ peptide with aaWr(l)* in either epitope and its percentage ratio in parentheses.
c) Number of fibrils that contain at least one Aβ peptide with Ewr(l)* (the Ewr(l) value is above the 95th percentile) with its percentage ratio among the fibrils in parentheses. In the third column, the number of fibrils that contain at least one Aβ peptide with Ewr(l)* in either epitope and its percentage ratio in parentheses.
d) Number of fibrils that contain at least one Aβ peptide with aaWr(l)* or Ewr(l)* with its percentage ratio among the fibrils in parentheses. In the third column, the number of fibrils that contain at least one Aβ peptide with aaWr(l)* or Ewr(l)* in either epitope and its percentage ratio in parentheses.

Identification of Aβ fragments across fibrils characterised by either aaWr(l)* or $E_{wr}(l)$*

We explored where the geometrically distinct fragments are located in Aβ peptides across polymorphic fibrils, which are characterised by either aaWr(l)* or $E_{wr}(l)$*. In this analysis, we used multiple window sizes, ranging from 4 to 10 Aβ residues.

First, we collected aaWr(l) values for the fragments in all the Aβ peptides across 69 fibrils using window sizes ranging from 4 to 10, which we referred to as the Starting Fragment Set (SFS), as shown in Fig. 5a. We calculated $E_{wr}(l)$ for the fragments in different window sizes for each Aβ peptide. In this analysis, using a higher number of aaWr(l) values collected with a range of window sizes compared to a single window size, we redefined aaWr(l)* as being $\geq \max(\text{aaWr}(l)) - h$, where h is the bin width determined using the Freedman–Diaconis rule[29], which is defined as

$$h = \frac{2\mathrm{IQR(SFS)}}{\sqrt[3]{n}} \quad (4)$$

where IQR(SFS) is the interquartile range of data in the SFS and n is the number of fragments collected in the SFS. The n value varied depending on the length of Aβ peptides in each fibril. The bin width h was also applied to calculate $E_{\mathrm{wr}}(l)$*.

We classified the fragments in the SFS with aaWr(l)* and $E_{\mathrm{wr}}(l)$* into four groups (Fig. 5a):

- W: fragment with aaWr(l)* (high writhe)
- U: fragment with $E_{\mathrm{wr}}(l)$* (high uniqueness)
- WU: fragment with both aaWr(l)* (high writhe) and $E_{\mathrm{wr}}(l)$* (high uniqueness)
- N: fragment with neither aaWr(l)* nor *E*wr(l)*

To select geometrically outlying fragments (Fig. 5a), we chose W1 and W2 fragments with the highest and the second highest aaWr(l)*, respectively, in the W group; U1 and U2 fragments with the highest and the second highest $E_{\mathrm{wr}}(l)$*, respectively, in the U group; and WU1 and WU2 fragments with the highest and the second highest aaWr(l)*, respectively, in the WU group.

Figure 5b shows the locations of the geometrically outlying WU1/WU2 (purple), W1/W2 (blue), and U1/U2 (red) fragments, plotted on the Aβ peptides across the 69 fibrils. We compared the fragment locations in the Aβ sequence with the reported epitopes for the four second-generation mAbs (Fig. 5c). The geometrically outlying regions identified using the two geometric measures mostly cover the reported epitope in the middle part of the Aβ sequence, while the geometrically outlying regions identified in the N-terminus of some fibrils are involved in the reported N-terminal epitopes (Fig. 5c). This result suggests that the conformational epitopes are characterised by the geometric measures aaWr(l)* and $E_{\mathrm{wr}}(l)$*.

The Aβ peptide in some fibrils has a geometrically outlying fragment in its C-terminal region (Fig. 5c), as seen in fibril 2lmo (9–40). These fragments are supposed to be potential conformational epitopes, although no mAbs have been reported to recognise the C-terminal part of Aβ in a fibril. Locating the potential conformational epitope at the C-terminal part of Aβ is also suggested by the averaged absWr(l) profile (Fig. 3c).

a

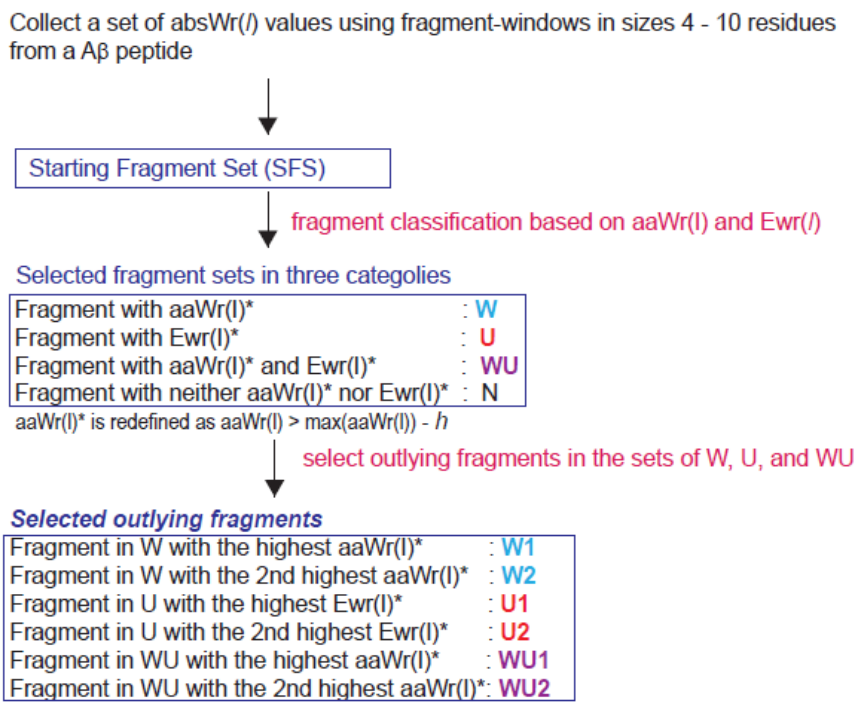
Collect a set of absWr(I) values using fragment-windows in sizes 4 - 10 residues from a Aβ peptide
Starting Fragment Set (SFS)
fragment classification based on aaWr(I) and Ewr(I)
Selected fragment sets in three categolies
Fragment with aaWr(I)* : W
Fragment with Ewr(I)* : U
Fragment with aaWr(I)* and Ewr(I)* : WU
Fragment with neither aaWr(I)* nor Ewr(I)* : N
aaWr(I)* is redefined as aaWr(I) > max(aaWr(I)) - h
select outlying fragments in the sets of W, U, and WU
Selected outlying fragments
Fragment in W with the highest aaWr(I)* : W1
Fragment in W with the 2nd highest aaWr(I)* : W2
Fragment in U with the highest Ewr(I)* : U1
Fragment in U with the 2nd highest Ewr(I)* : U2
Fragment in WU with the highest aaWr(I)* : WU1
Fragment in WU with the 2nd highest aaWr(I)* : WU2

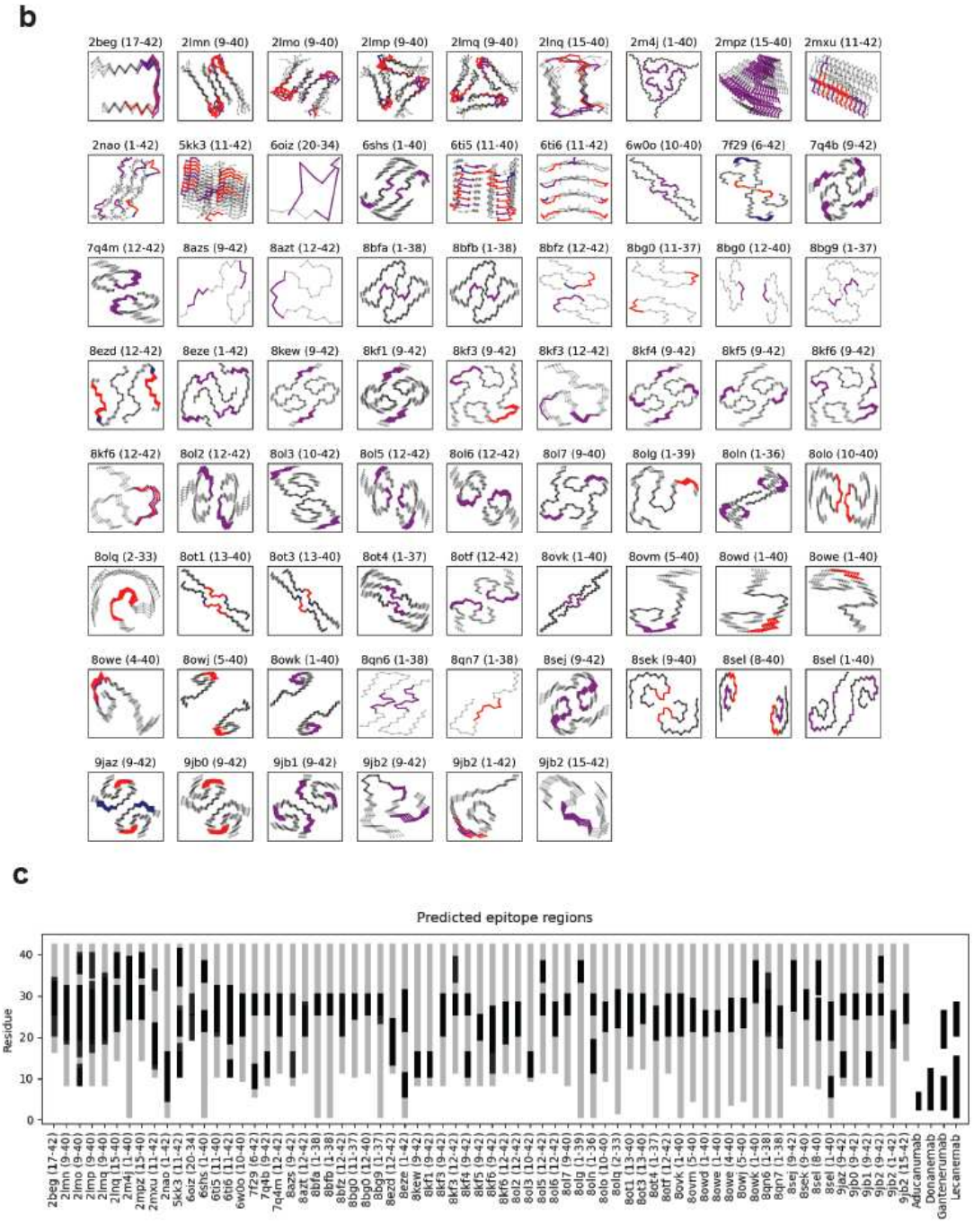

Fig. 5. Selecting geometrically distinct regions in Aβ. (**a**) Classification of the Aβ fragments in window sizes ranging from 4 to 10 based on the geometric measures absWr(l)* and $E_{wr}(l)$*; the geometrically outlying fragments labelled as W1, W2, U1, U2, WU1, and WU2, were selected. (**b**) Mapping geometrically outlying fragments on the Aβ sequences across 69 fibrils. The colours are assigned as follows: W1/W2 (blue), U1/U2 (red) and WU1/WU2 (purple). (**c**) Sequence positions of geometrically outlying fragments on the Aβ sequences across 69 fibrils (black bars). The reported sequences for the four second-generation mAbs are shown as vertical bars on the right side of the graph. Aβ: amyloid β.

Closer inspection of the results showed that the geometrically outlying fragments are located on Aβ structures close to the reported epitopes (Fig. 6a). The results indicate that the geometric outlying fragments in Aβ constitute the conformational epitopes.

Interestingly, Aβ peptides in some fibrils contain geometrically outlying fragments within the fibril structure (Fig. 6b). These epitopes in these fibril forms presumably hinder mAbs' access to epitopes, thereby impairing the therapeutic effect against these fibrils.

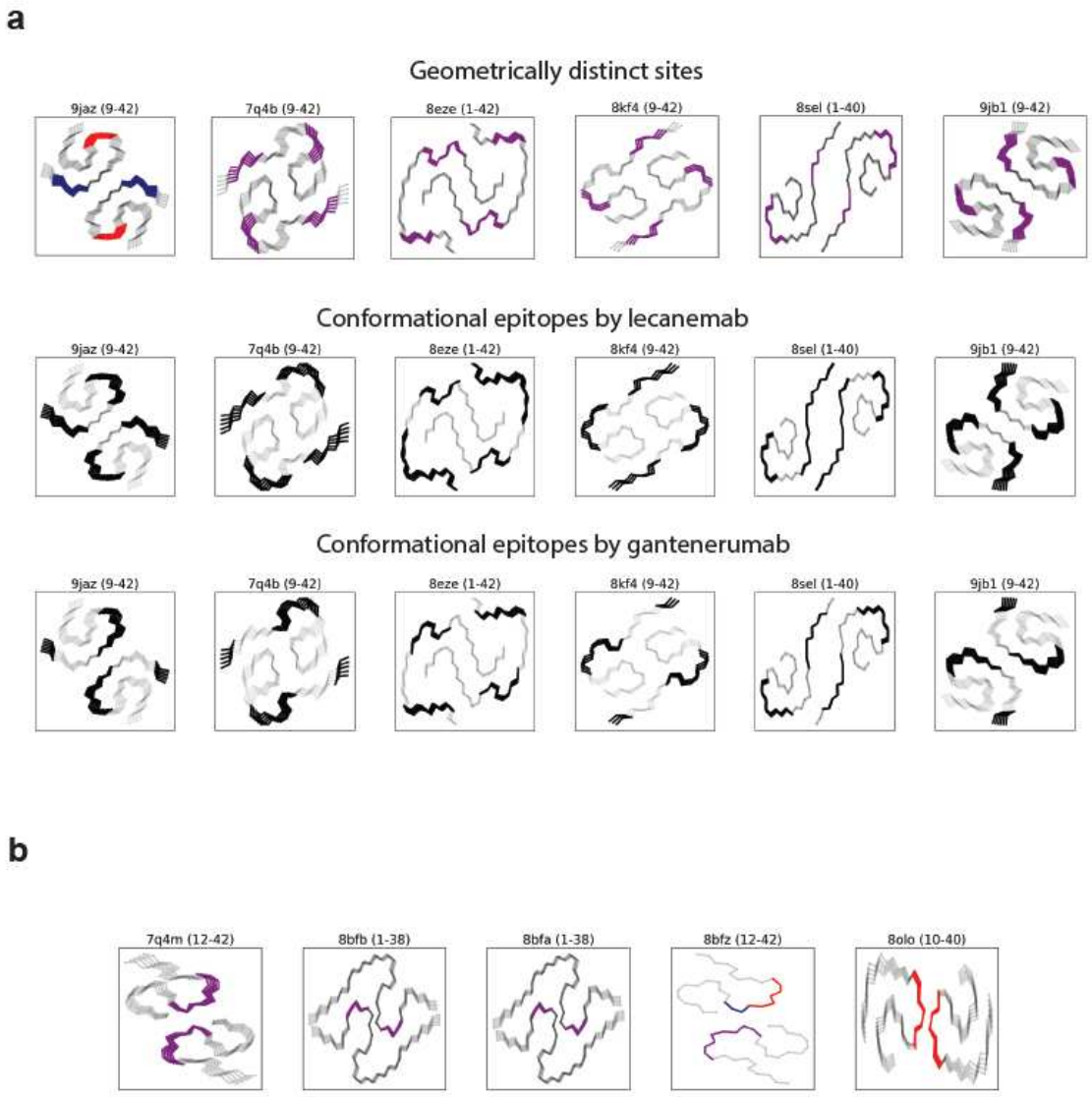

Fig. 6. Potential conformational epitopes identified by the geometric measures. (**a**) Comparing the locations of geometrically outlying fragments on Aβ sequences with the reported sequences of lecanemab (21–29) and gantenerumab (18–27) epitopes. (**b**) Aβ structures that have geometrically outlying fragments within the fibril structures. The colour usage for the geometrically marked segments is the same as in Fig. 5b. Aβ: amyloid β.

Discussion

In this work, we geometrically characterised conformational epitopes targeted by second-generation anti-Aβ mAbs using the writhe numerical measure[30]. We introduced two geometric measures, the average absolute local writhe, aaWr(l), and the local writhe energy, E_{wr}(l). Our main finding is that conformational epitopes exhibit distinctive geometric features: they have exceptionally high aaWr(l) and/or E_{wr}(l) values relative to other regions of Aβ in various fibrils. The aaWr(l) value indicates the degree of entanglement of a local Aβ structure, while E_{w}(l) increases when the fragment takes a geometry dissimilar to the other parts (geometric uniqueness). The findings suggest that second-generation mAbs (aducanumab, lecanemab, donanemab, and gantenerumab) preferentially recognise segments with distinct geometric features displayed on fibrils, thereby limiting distraction by the abundant monomeric Aβ species[11]. This may explain the improved efficacy of second-generation mAbs in removing pathogenic Aβ aggregates compared to first-generation mAbs[4-6].

A lack of understanding of the structural features of conformational epitopes hinders the development of an effective immunogen that accurately displays those epitopes as they appear in pathogenic Aβ species[9]. The geometric features of the conformational epitopes in fibrils, which were revealed in this work, will guide the design of an appropriate scaffold to present immunogenic Aβ fragments. The polymorphism of Aβ fibrils poses another fundamental obstacle to AD immunotherapy, which impairs the effectiveness of mAbs targeting fibrils[9,31]. Antibodies generated against an immunogen specific to a particular epitope conformation in a fibril may not bind to fibrils in different forms. Identifying potential conformational epitopes by their geometric features in various fibril forms helps elucidate how an anti-Aβ mAb works against a polymorphic set of Aβ fibrils formed in the brains of AD patients[6,7,28,32]. In this study, mapping the potential conformational epitopes in fibrils revealed differences in epitope accessibility across fibril forms (Figs. 5b and 6b), which is related to the efficacy of an mAb against polymorphic Aβ fibrils. Some fibrils hide the epitopes inside the fibrillar structures (Fig. 6b), which limits mAbs' access to the epitopes, reducing their efficacy. On the other hand, other fibril forms display two discrete epitopes on the same side of the fibril surface (Fig. 6a); these fibrils have high avidity to mAbs through cooperative binding of the two discrete epitopes. Mapping the potential conformational epitopes provides insights into how polymorphic Aβ fibrils impede AD immunotherapy with mAbs.

Molecular dynamics (MD) simulations of soluble Aβ oligomers and fibrils have been used to predict epitopes[9,33]. MD simulations identify epitopes as selectively exposed regions on oligomers or the weakest structural parts in fibrils, which become disordered and exposed on the fibril surface[9]. In those works, epitopes are assumed to be essentially unstructured and exposed on the surface of structured oligomers and fibrils, making them accessible to mAbs. In contrast to MD-based predictions, we assumed that conformational epitopes keep distinct geometric features displayed on fibril surfaces, which are explicitly recognised by second-generation mAbs. The distinct geometric features should be a primary determinant of the conformational epitope located in the middle part of Aβ in fibrils, as for lecanemab (21–29) and gantenerumab (18–27). The epitopes at the N-terminus of Aβ are not supposed to keep specific conformations in most fibrils, as evidenced by the lack of experimentally determined N-terminal segments (Fig. 5c). The N-terminal epitopes in such fibril forms are exposed to the solvent, and their sequences are recognised by mAbs. The conformational epitopes in the N-terminal and middle parts of Aβ should work differently in binding to mAbs. As shown by mapping the geometrically distinct parts of Aβ, the epitopes in the middle part should be recognised conformation-dependently by mAbs (Fig. 5c).

Geometric characterisation of proteins highlights distinct local structures that differ from those revealed by structural comparisons via coordinate overlay. We previously reported that geometrically distinct parts of a protein are frequently found at protein–protein interaction interfaces[14,15]. In this study, we found that conformational epitopes of Aβ in fibrils exhibit distinct geometric features, consistent with our previous results[14,15].

The reported epitope sequences targeted by the four second-generation mAbs are biochemically determined through enzyme-linked immunosorbent assays (ELISAs). In ELISA, Aβ fragments are used to identify the sequences recognised by the antibody fixed on a plate[34]; therefore, ELISA does not provide conformational information about epitopes but only their sequences. This technical limitation explains why the epitopes determined using ELISA are close to, but not perfectly aligned with, the segments identified using aaWr(l) and/or $E_{wr}(l)$ values (Fig. 5c). The epitope sequences determined using ELISA do not contain C-terminal epitopes around residues 35–40 (Figs 3d and 5c). We believe the C-terminal epitopes should be functional, but ELISA cannot detect them because they lose the conformational properties required for epitope recognition.

This work used only Aβ fibril forms. Lecanemab, for example, has a higher affinity to protofibrils than to fibrils and can also recognise oligomers[5,7]. The structural coordinates of Aβ in protofibrils and oligomers are not available[35], which limits our approach to fibrils. We cannot describe how the geometric features found in fibrils relate to lecanemab binding to Aβ protofibrils and oligomers. The structural details of protofibrils and oligomers are expected to expand our geometric characterisation to other species of Aβ peptide aggregates.

In summary, conformational epitopes of Aβ exhibit distinctive geometric features across various fibril forms. Our geometric measures reveal visually unidentified structural features of conformational epitopes in polymorphic Aβ fibrils, related to mAb binding. The potential epitope locations identified as geometrically distinct sites are close to those determined biochemically. Mapping the potential epitopes suggests that polymorphism in Aβ fibrils alters mAbs' accessibility to the epitopes, possibly altering the clinical benefit of AD immunotherapy.

Methods

Protein structure approximation

Protein structure was represented by consecutive Cα atoms as a linear polygonal curve in three-dimensional space, approximating the protein backbone. The following Aβ fibril structure coordinates in PDB were used in this work: 2beg, 2lmn, 2lmo, 2lmp, 2lmq, 2lnq, 2m4j, 2mpz, 2mxu, 2nao, 5kk3, 6oiz, 6shs, 6ti5, 6ti6, 6w0o, 7f29, 7q4b, 7q4m, 8azs, 8azt, 8bfa, 8bfb, 8bfz, 8bg0, 8bg9, 8ezd, 8eze, 8kew, 8kf1, 8kf3, 8kf4, 8kf5, 8kf6, 8ol2, 8ol3, 8ol5, 8ol6, 8ol7, 8olg, 8oln, 8olo, 8olq, 8ot1, 8ot3, 8ot4, 8otf, 8ovk, 8ovm, 8owd, 8owe, 8owj, 8owk, 8qn6, 8qn7, 8sej, 8sek, 8sel, 9jaz, 9jb0, 9jb1, and 9jb2.

Local writhe, Wr(l)

Local writhe as defined in eq. (1) for a segment l was calculated for a polygonal curve representing Aβ structure in fibril using the program used in our previous work[15,36]. The obtained Wr(l) values are used for plotting the absWr(l) profile by sliding a segment l position along the Aβ sequence, and calculating aaWr(l), defined in eq. (2).

Local writhe energy, $E_{wr(l)}$

A set of absWr(l) values is collected for all the fragments in Aβ, by sliding a window segment l comprising a defined number of residues over the sequence. In the histogram of the collected absWr(l) data with a defined bin width, the number of fragments in the bin showing the highest count is defined as $N(H_{wr})$: the highest count bin should include the fragments in the least or no entangled local conformation. If the conformational epitope gives the value P to its absWr(l), the number of fragments in the bin covering the value P is defined as $N(P_{wr})$. Using the values, $N(H_{wr})$ and $N(P_{wr})$, the local writhe energy, $E_{wr(l)}$, is obtained from eq. (3).

References

1 Karran, E. & De Strooper, B. The amyloid hypothesis in Alzheimer disease: new insights from new therapeutics. *Nature Reviews Drug Discovery* **21**, 306–318, doi:10.1038/s41573-022-00391-w (2022).

2 Jansen, W. J. *et al.* Prevalence of Cerebral Amyloid Pathology in Persons Without Dementia. *JAMA* **313**, 1924, doi:10.1001/jama.2015.4668 (2015).

3 Long, J. M. & Holtzman, D. M. Alzheimer Disease: An Update on Pathobiology and Treatment Strategies. *Cell* **179**, 312–339, doi:10.1016/j.cell.2019.09.001 (2019).

4 Rafii, M. S. & Aisen, P. S. Amyloid-lowering immunotherapies for Alzheimer disease: current status and future directions. *Nature Reviews Neurology* **21**, 490–498, doi:10.1038/s41582-025-01123-5 (2025).

5 Kim, B.-H. *et al.* Second-generation anti-amyloid monoclonal antibodies for Alzheimer's disease: current landscape and future perspectives. *Translational Neurodegeneration* **14**, doi:10.1186/s40035-025-00465-w (2025).

6 Cummings, J., Osse, A. M. L., Cammann, D., Powell, J. & Chen, J. Anti-Amyloid Monoclonal Antibodies for the Treatment of Alzheimer's Disease. *BioDrugs* **38**, 5–22, doi:10.1007/s40259-023-00633-2 (2024).

7 Perneczky, R. *et al.* Anti-amyloid antibody therapies in Alzheimer's disease. *Brain* **146**, 842–849, doi:10.1093/brain/awad005 (2023).

8 Glabe, C. G. Conformation-dependent antibodies target diseases of protein misfolding. *Trends Biochem Sci* **29**, 542–547, doi:10.1016/j.tibs.2004.08.009 (2004).

9 Plotkin, S. S. & Cashman, N. R. Passive immunotherapies targeting Abeta and tau in Alzheimer's disease. *Neurobiol Dis* **144**, 105010, doi:10.1016/j.nbd.2020.105010 (2020).

10 Lue, L. F. *et al.* Soluble amyloid beta peptide concentration as a predictor of synaptic change in Alzheimer's disease. *Am J Pathol* **155**, 853–862, doi:10.1016/s0002-9440(10)65184-x (1999).

11 Yang, T., Li, S., Xu, H., Walsh, D. M. & Selkoe, D. J. Large Soluble Oligomers of Amyloid beta-Protein from Alzheimer Brain Are Far Less Neuroactive Than the Smaller Oligomers to Which They Dissociate. *The Journal of neuroscience : the official journal of the Society for Neuroscience* **37**, 152–163, doi:10.1523/JNEUROSCI.1698-16.2016 (2017).

12 Tycko, R. Amyloid Polymorphism: Structural Basis and Neurobiological Relevance. *Neuron* **86**, 632–645, doi:10.1016/j.neuron.2015.03.017 (2015).

13 Baldwin, Q., Sumpter, B. & Panagiotou, E. The Local Topological Free Energy of the SARS-CoV-2 Spike Protein. *Polymers* **14**, 3014, doi:10.3390/polym14153014 (2022).

14 Baldwin, Q. & Panagiotou, E. The local topological free energy of proteins. *J Theor Biol* **529**, 110854, doi:10.1016/j.jtbi.2021.110854 (2021).

15 Sugiyama, M., Kosik, K. S. & Panagiotou, E. Geometry based prediction of tau protein sites and motifs associated with misfolding and aggregation. *Scientific reports* **15**, 10283, doi:10.1038/s41598-025-93304-x (2025).

16 Katritch, V., Olson, W. K., Pieranski, P., Dubochet, J. & Stasiak, A. Properties of ideal composite knots. *Nature* **388**, 148–151, doi:10.1038/40582 (1997).

17 Katritch, V. *et al.* Geometry and physics of knots. *Nature* **384**, 142–145, doi:10.1038/384142a0 (1996).

18 Sleiman, J. L., Conforto, F., Fosado, Y. A. G. & Michieletto, D. Geometric learning of knot topology. *Soft Matter* **20**, 71–78, doi:10.1039/d3sm01199b (2023).

19 Sleiman, J. L., Burton, R. H., Caraglio, M., Gutierrez Fosado, Y. A. & Michieletto, D. Geometric Predictors of Knotted and Linked Arcs. *ACS Polymers Au* **2**, 341–350, doi:10.1021/acspolymersau.2c00021 (2022).

20 Kauffman, L. H. An invariant of regular isotopy. *Transactions of the American Mathematical Society* **318**, 417–471, doi:10.1090/s0002-9947-1990-0958895-7 (1990).

21 Alexander, J. W. Topological Invariants of Knots and Links. *Transactions of the American Mathematical Society* **30**, 275–306, doi:10.2307/1989123 (1928).

22 Cerf, C. & Stasiak, A. A topological invariant to predict the three-dimensional writhe of

ideal configurations of knots and links. *Proceedings of the National Academy of Sciences* **97**, 3795–3798, doi:10.1073/pnas.97.8.3795 (2000).
23 Panagiotou, E. & Plaxco, K. A topological study of protein folding kinetics. *Topology and Geometry of Biopolymers*, 223–234, doi:10.1090/conm/746/15010 (2020).
24 Wang, J. & Panagiotou, E. The protein folding rate and the geometry and topology of the native state. *Scientific reports* **12**, doi:10.1038/s41598-022-09924-0 (2022).
25 Bohrmann, B. *et al.* Gantenerumab: a novel human anti-Abeta antibody demonstrates sustained cerebral amyloid-beta binding and elicits cell-mediated removal of human amyloid-beta. *J Alzheimers Dis* **28**, 49–69, doi:10.3233/JAD-2011-110977 (2012).
26 Lord, A. *et al.* An amyloid-β protofibril-selective antibody prevents amyloid formation in a mouse model of Alzheimer's disease. *Neurobiology of Disease* **36**, 425–434, doi:https://doi.org/10.1016/j.nbd.2009.08.007 (2009).
27 Arndt, J. W. *et al.* Structural and kinetic basis for the selectivity of aducanumab for aggregated forms of amyloid-β. *Scientific reports* **8**, doi:10.1038/s41598-018-24501-0 (2018).
28 Zhang, Y., Chen, H., Li, R., Sterling, K. & Song, W. Amyloid β-based therapy for Alzheimer's disease: challenges, successes and future. *Signal Transduction and Targeted Therapy* **8**, doi:10.1038/s41392-023-01484-7 (2023).
29 Freedman, D. & Diaconis, P. On the histogram as a density estimator:L 2 theory. *Zeitschrift fr Wahrscheinlichkeitstheorie und Verwandte Gebiete* **57**, 453–476, doi:10.1007/bf01025868 (1981).
30 Fuller, F. B. The Writhing Number of a Space Curve. *Proceedings of the National Academy of Sciences* **68**, 815–819, doi:10.1073/pnas.68.4.815 (1971).
31 Scheres, S. H. W., Ryskeldi-Falcon, B. & Goedert, M. Molecular pathology of neurodegenerative diseases by cryo-EM of amyloids. *Nature* **621**, 701–710, doi:10.1038/s41586-023-06437-2 (2023).
32 Kollmer, M. *et al.* Cryo-EM structure and polymorphism of Aβ amyloid fibrils purified from Alzheimer's brain tissue. *Nature communications* **10**, doi:10.1038/s41467-019-12683-8 (2019).
33 Peng, X., Cashman, N. R. & Plotkin, S. S. Prediction of Misfolding-Specific Epitopes in SOD1 Using Collective Coordinates. *J Phys Chem B* **122**, 11662–11676, doi:10.1021/acs.jpcb.8b07680 (2018).
34 Englund, H. *et al.* Sensitive ELISA detection of amyloid-β protofibrils in biological samples. *Journal of Neurochemistry* **103**, 334–345, doi:https://doi.org/10.1111/j.1471-4159.2007.04759.x (2007).
35 Chen, G.-F. *et al.* Amyloid beta: structure, biology and structure-based therapeutic development. *Acta Pharmacologica Sinica* **38**, 1205–1235, doi:10.1038/aps.2017.28 (2017).
36 Sugiyama, M., Kosik, K. S. & Panagiotou, E. Mathematical topology and geometry-based classification of tauopathies. *Scientific reports* **14**, 7560, doi:10.1038/s41598-024-58221-5 (2024).

Acknowledgements
The start-up fund for M.S. from the WPI-SKCM^2 is appreciated. This project has been performed using the computer resources provided by the WPI-SKCM^2. We thank Elsevier Language Editing Services for editing a draft of this manuscript.

Author contributions
M.S. and S.T. conceived the project. M.S. conducted the calculation with the support of E.P. M.S. and S.T. analysed the results. M.S. and S.T. contextualised the results. All the authors, including M.S., S.H., E.P. and S.T., reviewed and edited the manuscript.

Funding
S.T. acknowledges the financial support from Grant-in-Aid for Scientific Research (B) (general) (23H02425) and Grant-in-Aid for Challenging Research (Pioneering) (21K18234) from JSPS KAKENHI. This work was partly supported by MEXT Promotion of Distinctive Joint Usage/Research Centre Support Program Grant Number JPMXP0724020292.

Data availability statement
All data generated or analysed during this study are included in this published article and supplementary material.

Competing interests
The authors declare no competing interests.

Additional information
There has been no significant financial support for this work that could have influenced its outcome.

Supplementary information: The online version contains supplementary materials.

Correspondence and requests for materials should be addressed to S.T.

Supplementary Files

This is a list of supplementary files associated with this preprint. Click to download.

- SupplementarymaterialFinal02a.pdf